Morphology of Poly(2-ethylhexyl methacrylate):Poly(butyl methacrylate) Latex Blend Films

Olga Vorobyova and Mitchell A. Winnik*

Department of Chemistry, University of Toronto, 80 St. George St., Toronto, Ontario, Canada M5S 3H6

Received June 22, 2000; Revised Manuscript Received December 6, 2000

ABSTRACT: This paper describes the morphology of the latex films formed from a mixture of two different latex particles: poly(butyl methacrylate) (PBMA, 120 nm) and poly(2-ethylhexyl methacrylate) (PEHMA, 100 nm). Twenty percent of the PBMA phase is labeled with 1 mol % anthracene. Using confocal fluorescence microscopy, we obtained images of the internal morphology of the dry films. Atomic force microscopy was used to image the surfaces of the films. For the same blend composition, 10 wt % PBMA and 90 wt % PEHMA, we studied the effect of two factors on the blend morphology: the presence or the absence of the surfactant SDS (ca. 2 wt % of the weight of polymers) in the dispersion and the dispersion concentration. We related the different morphologies we observed to the differences in the drying mechanisms. In the case of a surfactant-free film cast from a 5 wt % dispersion mixture, the film dried homogeneously, and we observed uniform distribution of the PBMA dispersed phase in the PEHMA matrix. In the presence of surfactant, the film dries laterally with a propagating drying front, and we observed network-like structures formed by PBMA particles in a matrix of PEHMA. The segregation of PBMA and PEHMA particles can be explained by differences in the surfactant adsorption onto PBMA and PEHMA particles.

Introduction

This paper is concerned with the morphology of films formed from a mixture of two different latex particles. When different colloidal species are mixed in a dispersion, they have the possibility of mixing uniformly or of undergoing partial or complete segregation. In addition, flocculation can occur, and the flocs can be enriched in one of the components. As the mixed dispersion dries to form a film, one imagines that the morphology in the film depends on the state of the mixture at high solids. While some scientists study bimodal colloidal blends in the dispersed state,[1] the more common situation is that one characterizes the morphology of the solid state and tries to infer from this morphology interactions that occurred in the dispersion at high solids.[2] Knowledge of the factors that control the latex blend morphology is particularly relevant for industrial coatings, which often have a number of additives, including inorganic pigments. Their distribution inside the film can affect the properties of coating. One can expect that the latex film structure will depend on the properties of the components, blend composition, and the drying conditions.

Our initial goal was to prepare blend films with a uniform distribution of ca. 10 wt % PBMA latex particles in a PEHMA matrix. These films were used to study shear-induced coalescence in PBMA:PEHMA blends.[3] Specific features of the instrument (the geometry of the sample chamber in the rheometer) set requirements on the thickness and size of the film that could be used (i.e., a disk-shaped film 25 mm in diameter and 0.4−0.5 mm in thickness). As a result, our film preparation procedure was geared to these requirements. When we found that there was a tendency for the PBMA particles to segregate in PBMA:PEHMA blend films, we decided to investigate this phenomenon. What follows is a description of the results obtained. Our objective was to identify some of the important variables affecting the blend morphology, rather than a definitive study of the particle segregation mechanism.

Traditionally, latex blend morphology is studied by such techniques as atomic force microscopy (AFM) and scanning electron microscopy (SEM). These techniques can provide information about the surface structure of the films but not about the morphology within the film. Thin sections or freeze fracture replicas can be examined by transmission electron microscopy (TEM)[4] to study film structure in the bulk of the film. These techniques are labor-intensive. Thin sections require staining for contrast. Identifying domain composition in freeze-fracture images is a difficult challenge. Here we employ laser scanning confocal fluorescence microscopy (LSCFM) as a noninvasive technique that allows one to perform a 3D profiling of a sample without microtoming. Confocal microscopy is a very powerful tool for the study of polymer blends[5] and was successfully used in the past to examine morphology of polymer latex films[6] and a trilayer polymer paint.[7] It can resolve features comparable in size with the wavelength of light.

Experimental Section

Latex Synthesis. Poly(2-ethylhexyl methacrylate) (PEHMA) and poly(butyl methacrylate) (PBMA) latex dispersions were prepared by two-stage seeded emulsion polymerization, with the fluorescent dye introduced during the second stage. The anthracene-labeled PEHMA latex and the unlabeled PEHMA latex were prepared by Pham.[8] Both the anthracene- and phenanthrene-labeled (1 mol % dye) PBMA dispersions were synthesized by Feng.[9] An important feature of the synthesis is that one must add more surfactant (sodium dodecyl sulfate, SDS) to the recipe for the preparation of PEHMA particles (2.3 wt %, based on total monomer) than for the preparation of PBMA particles (2.1 wt %). The size of the latex particles used in this study, and the molecular weight of their constituent polymers, are listed in Table 1.

* To whom correspondence should be addressed. E-mail: mwinnik@chem.utoronto.ca.

10.1021/ma001080u CCC: $20.00
Published on Web 02/23/2001

Table 1. Latex Characteristics

	fluorescent dye	diam (nm)	$10^{-3}M_w$[a]	$10^{-3}M_n$[a]
PBMA-Phe	phenanthrene	119	35.7	16.7
PBMA-An	anthracene	119	33.9	18.3
PEHMA		99	140	48

[a] Determined using PMMA standards in size exclusion chromatography measurements.

Sample Preparation. *Surfactant-Containing Films Cast from 30 wt % Dispersion* The following blend composition was used throughout all the experiments: PEHMA:PBMA-Phe:PBMA-An 9:0.8:0.2.[10] Known amounts of PEHMA and PBMA dispersions were mixed to give the blend composition of 90 wt % PEHMA and 10 wt % PBMA. The mixture (8 mL) was degassed by subjecting it to low pressure, cast onto a freshly cleaved mica sheet 8 × 8 cm, and then left overnight to dry uncovered at ambient conditions (23−25 °C, relative humidity (RH) 50−60%). The film preparation procedure described above was designed to produce rather thick films quickly and efficiently to use in rheometer experiments. The uniformity of film thickness and mechanical strength (i.e., the history of the film) were not thought to be important because, in the rheometer, the film was to be heated at a temperature much higher than the glass transition temperature of the blend components and gently compressed between the cone and the plate. To obtain a thick and uniform film, one should slow the drying rate by covering the film, so that the humidity around the film remains close to 100%. Then film drying would take place over a period of several days.

Surfactant-Free Films In some experiments, before casting films, the latex mixture was diluted to yield a 5 wt % dispersion and treated with a prepurified ion-exchange resin (Bio-Rad mixed-bed resin AG 501-X8) to remove the sodium dodecyl sulfate (SDS) surfactant and other low molecular weight inorganic compounds used in the latex synthesis. In that case, the mixture was twice stirred for 2 h with a fresh portion of the resin, added in the amount of 20 wt % of the total latex solids. The resin beads were filtered out, and the film preparation was carried out as described above. The dry films were clear with a uniform thickness of ca. 200 μm.

Surfactant-Containing Films Cast from 5 wt % Dispersion Individual latex dispersions were diluted from 30 to 5 wt % solids content. The diluted dispersions were mixed to produce the desired blend composition. The mixture was degassed by subjecting it to low pressure and cast on a clean quartz plate 1 × 2 cm. The dispersions were allowed to dry uncovered at ambient conditions (23−25 °C, RH 50−60%). The dried films had a "stadium" structure, with a thick rim of 1.5−2 mm in width surrounding a flat interior, approximately 20 μm thick. Most of the film material (ca. 60%) was located in the rim with the maximal thickness of ca. 60 μm. The films were clear and showed no signs of cracking.

Laser Scanning Confocal Fluorescence Microscopy (LSCFM). A Zeiss LSM 510 confocal instrument with a water immersion C-Apochromat 63x/1.2w corrected objective was used. Anthracene was excited with the 364 nm band of a Coherent Enterprise ENTC-635 laser. A 385 nm cutoff filter was used to prevent the excitation light from reaching the detector. The confocal pinhole was set at 79 μm, which corresponds to an optical slice thickness of 0.6 μm.

Image analysis software AIS from Imaging Research Inc. was used to estimate the size of the PBMA droplets. The following parameters were selected to characterize the PBMA phase: the average particle diameter, the fraction of the image occupied by the PBMA phase, and the number of PBMA droplets detected. Before proceeding with the image analysis, the images were binarized and filtered. (The objects smaller than 4 pixels in size were removed from the image.) The data were obtained by averaging the results of the analysis of at least 10 different optical sections. The thickness of the optical slice is 0.6 μm, which is comparable to the size of the droplets detected. In that case, we can assume that there is no significant truncation of the particles or that the fraction of the truncated profiles (with radius $r < R_{true}$) is small. This assumption allows us to use the average profile diameter as a measure of the true particle diameter without any additional treatment.

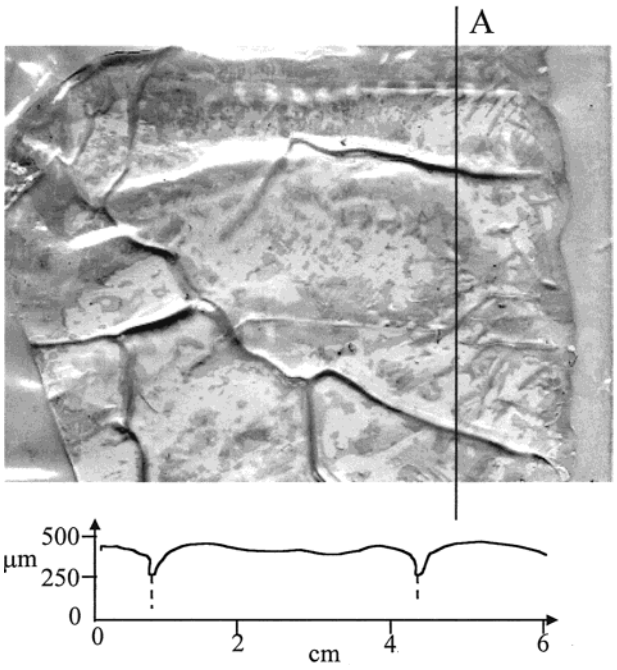

Figure 1. Top: a top view of freshly formed surfactant-containing film PEHMA:PBMA 9:1 prepared from a 30 wt % dispersion. Image size: 6 × 9 cm. Bottom: an estimated film thickness profile along line A.

Atomic Force Microscopy (AFM). AFM images of latex films surfaces were obtained with Nanoscope III (Digital Instruments, Santa Barbara, CA) using silicone nitride tips. The images were obtained in the contact mode.

Results

All of our experiments were carried out on blends containing 90% PEHMA, 8% phenanthrene-labeled PBMA, and 2% anthracene-labeled PBMA. Since the two polymers have densities very close to 1.0, the amounts mentioned refer both to weight percent and to volume percent. In fluorescence microscopy experiments, only the anthracene groups can be detected.

Our initial experiments were carried out on latex film samples prepared by mixing surfactant-containing dispersions at 30 wt % solids and then casting films onto freshly cleaved mica sheets, 8 × 8 cm. The films were then left overnight to dry uncovered at ambient conditions. These films dried from the edges inward. Soon after the drying started, a skin of coagulated particles was seen on the surface of the dispersion. Most of the film became clear in about 6 h, but additional time was necessary for the turbid spot in the center of the film to become clear. The total drying time was about 8−10 h. The dry film had an uneven thickness: during final stages of drying, cracks were formed that are seen as dark lines randomly crossing the film in Figure 1. These cracks are partially healed in the dry film, so that the film can be lifted off the substrate as a single piece. The film thickness varied throughout the film with a maximum thickness of 0.5 mm. The edges of the film were somewhat thinner. The average thickness was 0.4 mm. Figure 1 shows an image of the dry film and the estimated thickness profile with the cracks that can be seen clearly. The morphology of these films, at high

magnification, was examined by atomic force microscopy and by laser scanning confocal fluorescence microscopy.

Structure of Film Surfaces Studied with Atomic Force Microscopy. AFM is a powerful technique for surface characterization, which is now well-established for latex film studies.[11−13] It can resolve objects on a nanometer scale, thus enabling one to study fine details of the surface structure. We use AFM as a technique complementary to confocal microscopy in the study of PBMA:PEHMA blends. Both film surfaces were examined by AFM: the air surface (air−polymer interface) and the mica surface (polymer−substrate interface). To examine the mica surface, we were able to pull the relatively thick films (0.4−0.5 mm) slowly from the substrate with a forceps, taking care not to stretch the films. All the images were obtained in the contact mode, which shows only the topography of the surface but does not provide information about the chemical species involved. However, we are able to make phase assignments based on the difference in the glass transition temperature of the components. PEHMA is much softer than PBMA and completely interdiffuses, forming a continuous matrix. PBMA latex particles, on the other hand, remain as separate entities.

Both the PEHMA and PBMA latex contain a small amount of surfactant, sodium dodecyl sulfate (SDS, ca. 2 wt % of the weight of the polymer), added during the emulsion polymerization. Other inorganic materials such as salts used as pH buffers and initiator fragments were also present in the latex dispersion and are carried into the film. These substances present in the raw latex can interfere with our analysis of the surface film morphology. There is evidence in the literature that these materials tend to accumulate at the film surfaces.[11−14] To examine the effect of surfactant on the surface structure in PBMA−PEHMA blends, we examined three different films: a surfactant-free film prepared from an ion-exchanged dispersion, a surfactant-containing film, and a surfactant-containing film that was soaked in water for 10 min. Figures 2−4 show AFM images of these films.

The air surface of a surfactant-free film (Figure 2A) has a considerable roughness, compared to the other much smoother surface that was in contact with the mica (Figure 2B). The air surface of a surfactant-containing film prepared from a 30 wt % dispersion is not as rough, as shown in Figure 3A. The mica surface of a surfactant-containing film, however, shows a number of very sharp peaks that can be seen in Figure 3B. These peaks may be due to surfactant or caused by the pullout of the soft PEHMA from the mica surface when the film was peeled from mica. Note that these peaks are not present in the corresponding image of the surfactant-free film (Figure 2B).

When a surfactant-containing film was soaked in water for 10 min, the film changes in appearance from completely transparent to opaque white, and we observe a remarkable change in the image of the mica surface of the film (Figure 4B). Where there were sharp peaks before contact with water, we now see a pattern of holes in the film surface. When a surfactant-containing film is immersed in water, the surfactant and other water-soluble inorganic materials dissolve and are washed away from the surface. The phenomenon of water absorption by surfactant-containing latex films was studied in detail by Agarwal and Farris,[15] who suggest that upon drying there are traces of surfactant left in

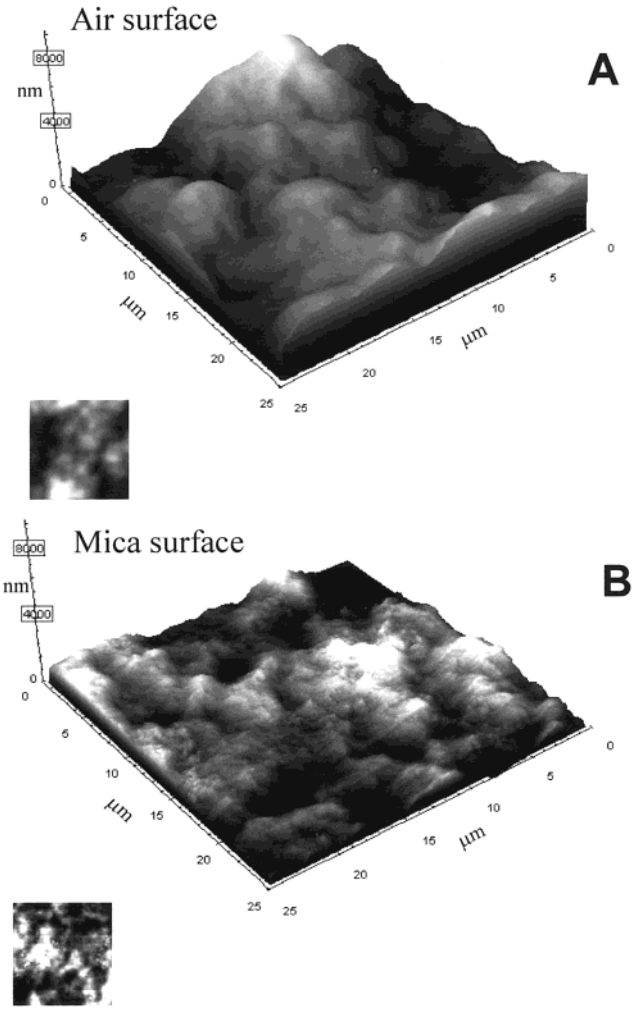

Figure 2. AFM images of a freshly formed surfactant-free film PEHMA:PBMA 9:1 prepared from a 5 wt % dispersion: (A) air surface; (B) mica surface.

the channels that served as conduits in the wet film for water evaporation and surfactant exudation to the film surface. These channels are recreated as water diffuses into the dry film. The micron-size holes seen in Figure 4B may not represent channels filled by the surfactant in the dry film. Rather, on the basis of Agarwal and Farris conclusions,[15] we attribute them to water penetrating into the film under osmotic forces to dissolve surfactant trapped within the film. PEHMA, which is quite soft at room temperature, yields and makes room for the water, creating holes in the film.

The image of the air surface of the washed film is not so different, however, from what we observed for surfactant-containing and surfactant-free films (compare Figure 4A and Figures 2A and 3A). The image in Figure 4A is somewhat smoother, which may be an effect of the higher magnification in this image. (Note that this image is 10 × 10 μm, while all of the other images in Figures 2−4 are 25 × 25 μm.) However, the air surface images of surfactant-containing and surfactant-free films are also very similar. This fact, together with the absence of any new features in the image of a washed film, tells us that there is little exudation of surfactant to the air surface of these films, compared to the extent of surfactant exudation to the mica surface.

The images presented in Figures 2−4 provide relatively low-resolution views of global film topography. At

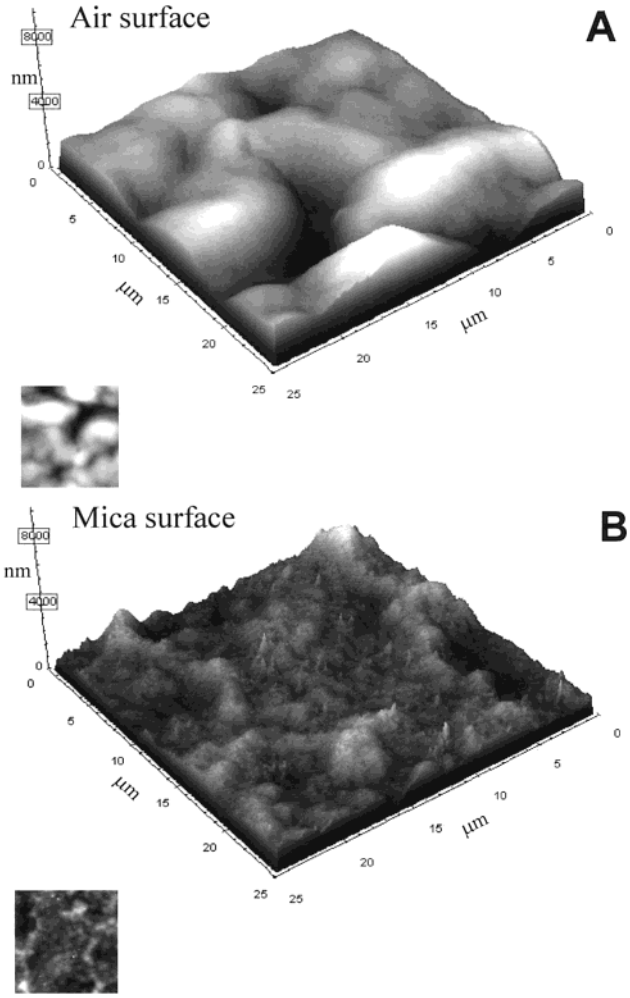

Figure 3. AFM images of a freshly formed surfactant-containing film PEHMA:PBMA 9:1 prepared from a 30 wt % dispersion: (A) air surface; (B) mica surface.

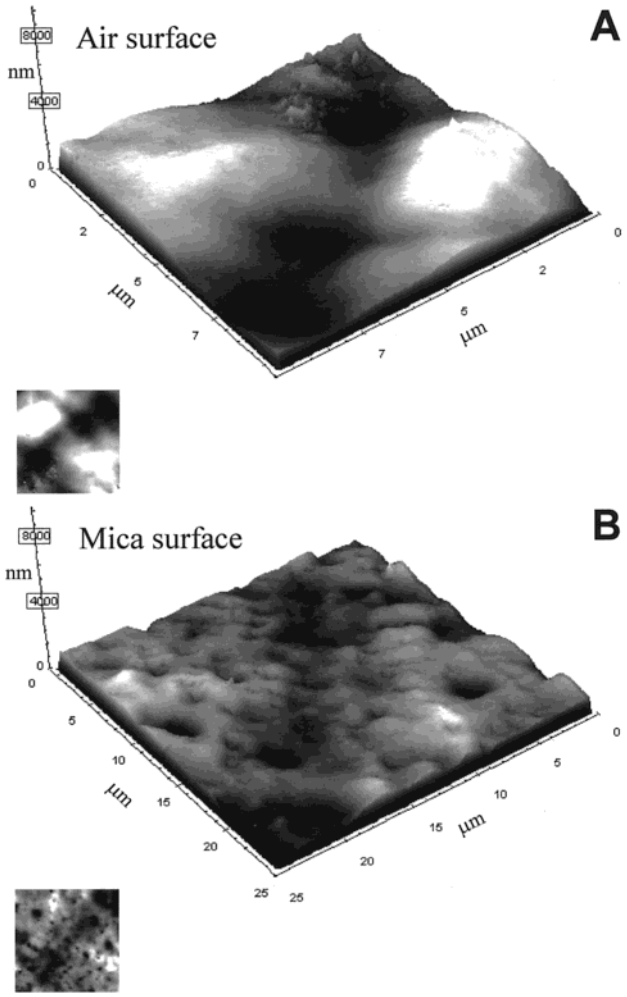

Figure 4. AFM images of a water-washed surfactant-containing film PEHMA:PBMA 9:1. The film was prepared from a 30 wt % dispersion and then soaked in water for 10 min: (A) air surface; (B) mica surface.

this level of resolution, individual latex particles (ca. 0.1 μm diameter) cannot be resolved. Images obtained at higher magnification provide information about the distribution of the hard PBMA particles in the softer PEHMA matrix. Figure 5 shows a higher resolution image of the film shown in the top of Figure 3, a 5 $\times$ 5 μm image of the air surface of the surfactant-containing film cast from a 30 wt % dispersion. We note that in this image the local surface roughness is not very large; on average, it corresponds to 500 nm, which is the size of five PEHMA particles. Also, we observe the presence of many tiny bumps on the film surface.

In Figure 6, which is a top view of the image in Figure 5, these bumps are seen as tiny white circles spread throughout the film surface. Figure 6 also shows a height profile along a line drawn randomly on the surface. The profile in Figure 6 allows us to determine the size and height of these objects. The profile in Figure 6 follows the topology of the surface: for example, for the first 2 μm along the line there is a gradual decline in the surface height. In this region, the profile also shows the presence of four peaks corresponding to four white circles in the top image in Figure 6. These peaks seem to be identical in size, with a height of ca. 50 nm and a width of ca. 150 nm. Figure 7 shows a close-up of the group of particles taken from Figure 6. The size of these objects (150 nm) corresponds to the size expected

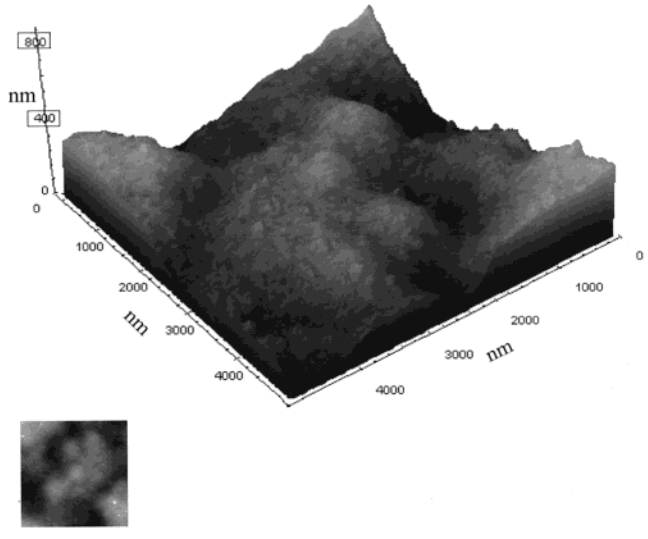

Figure 5. An AFM image of a freshly formed surfactant-containing film PEHMA:PBMA 9:1 prepared from a 30 wt % dispersion (air surface).

for the PBMA particles (120 nm diameter), embedded in the PEHMA matrix and convoluted with an AFM tip. From this analysis we identify the white circular objects seen in Figure 6 as PBMA particles.

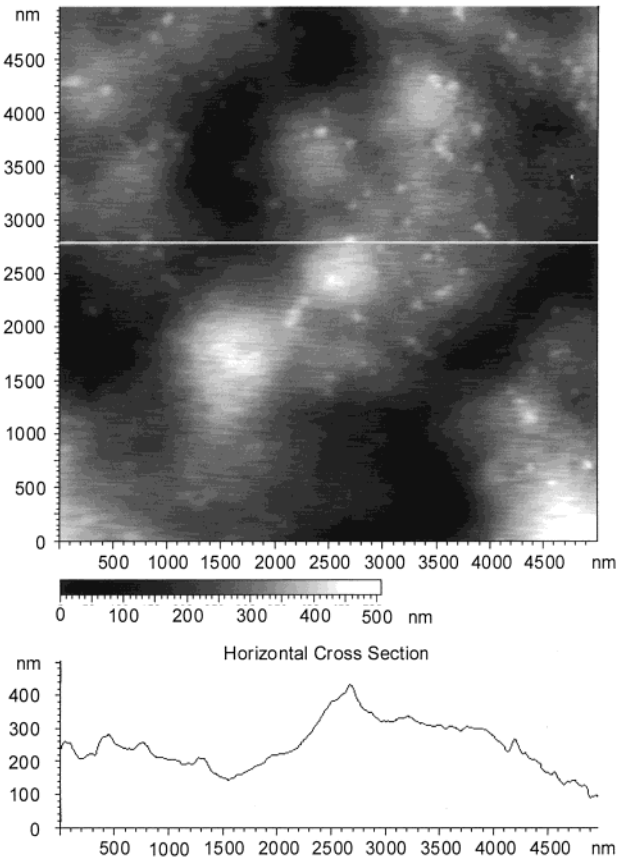

Figure 6. An AFM image of a freshly formed surfactant-containing film PEHMA:PBMA 9:1 prepared from a 30 wt % dispersion (air surface). A top view of the image in Figure 5.

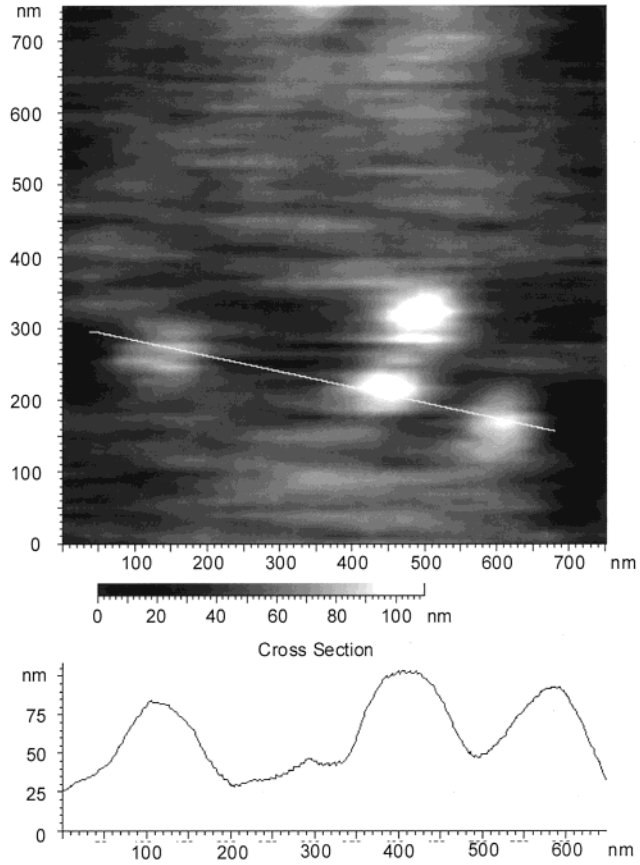

Figure 7. An AFM image of a freshly formed surfactant-containing film PEHMA:PBMA 9:1 prepared from a 30 wt % dispersion (air surface). A close-up from the image in Figure 6.

We found that a deflection AFM image (Figure 8) of the same film described above provides us with the best contrast to study the particle distribution. Figure 9 shows a 5 × 5 μm deflection AFM image of the air surface of a surfactant-free film. Although the contrast is poorer than in Figure 8, we still can detect a number of particles similar to those seen in Figure 8.

From the image in Figure 8 we can draw some interesting conclusions about the distribution of PBMA phase on the film surface. First of all, this particular region of the film surface seems to be enriched in the PBMA phase. For an area of 25 μm^2 and a volume fraction of the dispersed phase of 0.1, there should be 55 PBMA particles present. Instead, the total count in Figure 8 is 120. A second feature to which we draw attention is that the distribution of particles is nonuniform. Some areas are devoid of PBMA. Other areas display many PBMA particles in a loose cluster. Many of the PBMA particles in the image in Figure 8 have neighbors forming doublets, triplets, and other groups. Only one-third of the particles can be termed as singlets. Even when aggregated, these particles retain their individuality. No coalescence of PBMA occurred under the film formation conditions that we used.

Conclusions Based upon AFM. The examination of mica surfaces and air surfaces of PBMA−PEHMA films cast from surfactant-containing dispersions reveals that the surfactant SDS accumulated on the mica surface, whereas the air surface of the film seems to be surfactant-free. Higher magnification images of the film−air surface show PBMA particles embedded in a PEHMA matrix. We observed enrichment of the surface with

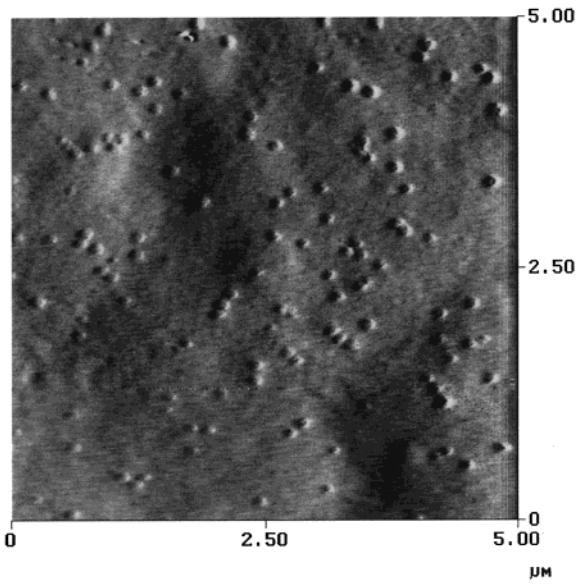

Figure 8. A deflection AFM image of a freshly formed surfactant-containing film PEHMA:PBMA 9:1 prepared from a 30 wt % dispersion (air surface). A top view of the image in Figure 5.

PBMA particles, which are present in larger quantities than one would expect from the blend composition. Also, the distribution of the PBMA particles is nonuniform, with many particles aggregated into loose clusters.

Depth Profiling with Confocal Fluorescence Microscopy. *Morphology of Surfactant-Containing*

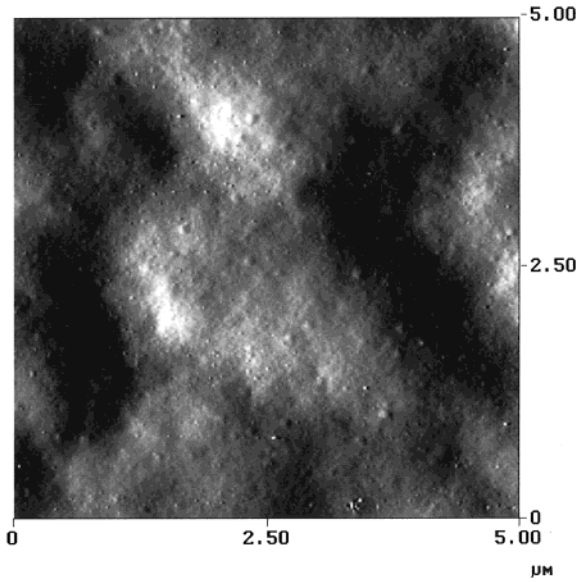

Figure 9. A deflection AFM image of a freshly formed surfactant-free film PEHMA:PBMA 9:1 prepared from a 5 wt % dispersion (air surface).

Blend. First, we describe the results obtained with a mixture of two surfactant-containing latex dispersions, each with a solids content of 30 wt %. The mixture of PEHMA and PBMA latex was cast onto a square sheet of mica 8 × 8 cm and was allowed to dry uncovered under ambient conditions. The ratio of dry PEHMA to PBMA was equal to 9:1 by weight.

The interior morphology of these films was studied by confocal fluorescence microscopy. Recall that one of every five PBMA latex particles in the blend is labeled with anthracene, providing us with the contrast necessary to distinguish between the PBMA and PEHMA phases. A stack of images at regular intervals was collected and used to represent the film structure at different depths, from the surface of the film to 100−150 μm inside the film. Figure 10 shows a selection of the images obtained with a freshly formed film. The first image in the series shown in Figure 10 corresponds to the image of the film surface ($Z = 0$ μm), and the rest of the images are obtained at a distance Z ranging from 10 to 41 μm from the surface. One can see that in the surface image there is a weblike pattern of white lines about 1 μm thick on a dark background. This web disappears in the next image (at 10 μm deep), which is uniformly gray. As we probe deeper inside the film, the network reappears. Many films have been examined in this way; this behavior is reproducible.

We interpret the formation of the network as evidence of the aggregation of PBMA particles during film drying. The small size of PBMA latex (120 nm) does not allow us to image the individual particles, so that from the confocal microscopy results only we cannot comment on the extent of this aggregation. However, we can presume that PBMA particles are spatially correlated in the film: a given PBMA particle is more likely to be surrounded by other PBMA particles than isolated in the PEHMA matrix.

Figures 11 and 12 show the images of the blend annealed at 100 °C for 1 and 3 h, respectively. We

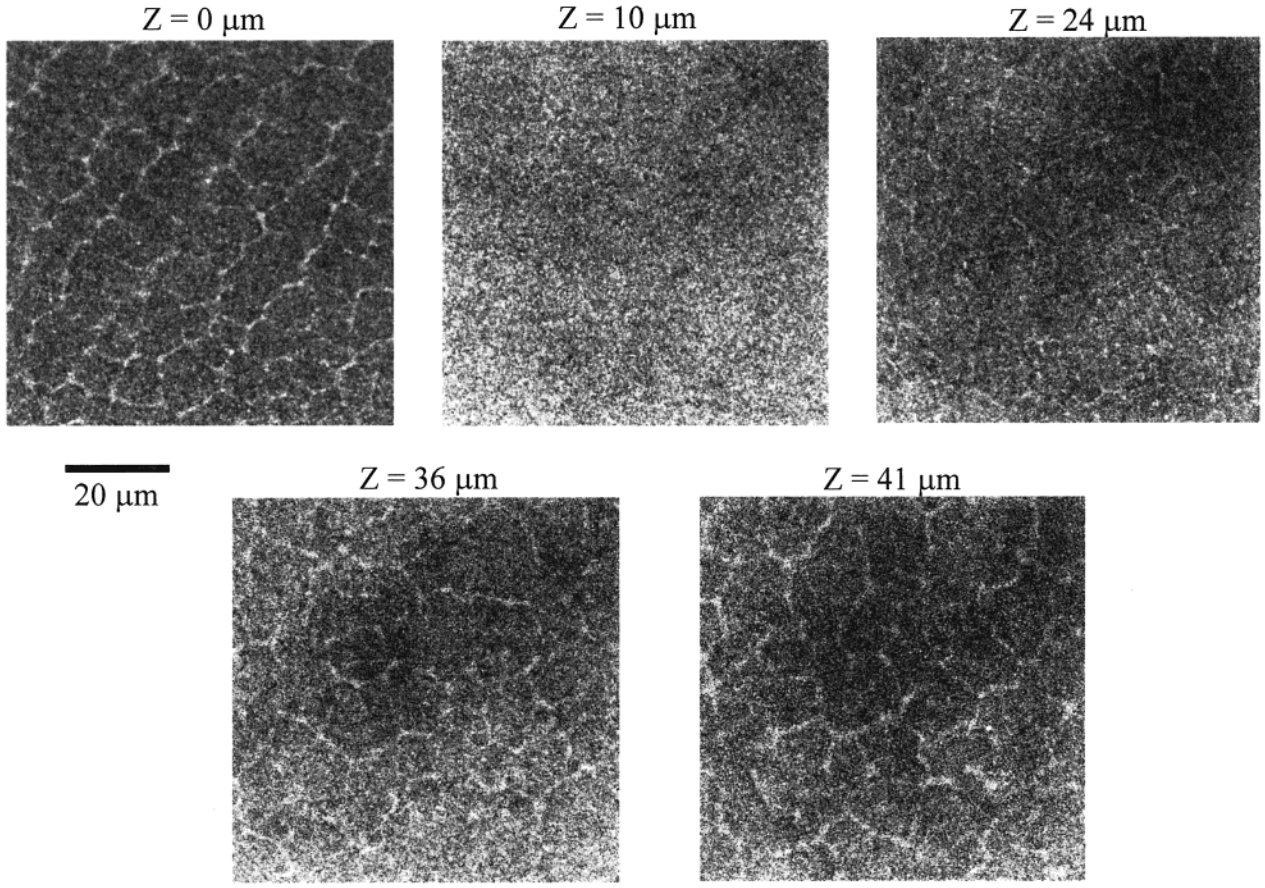

Figure 10. Confocal microscopy images of a freshly formed surfactant-containing film PEHMA:PBMA 9:1 prepared from a 30 wt % dispersion. Z is the distance from the surface. The image size is 73 × 73 μm.

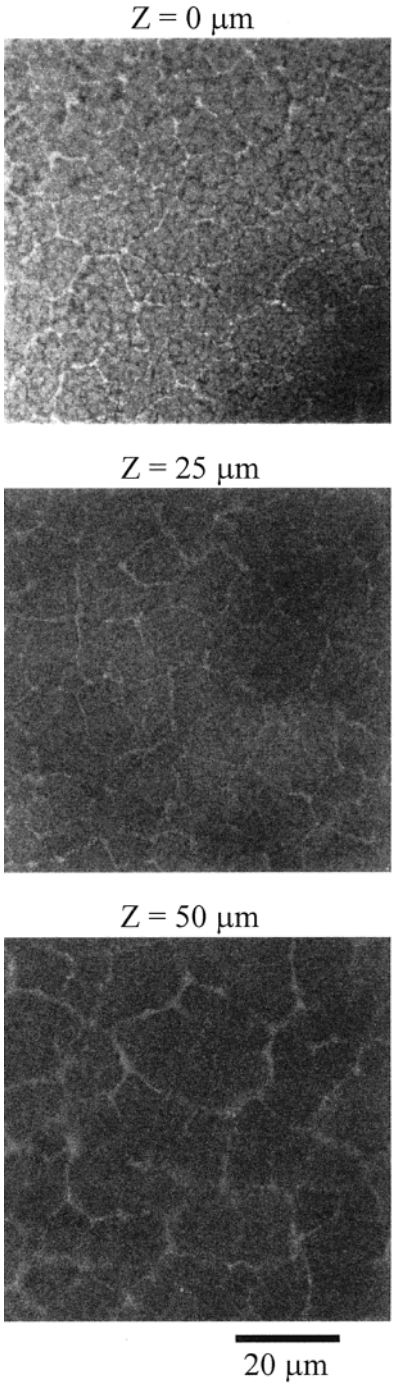

Figure 11. Confocal microscopy images of a surfactant-containing film PEHMA:PBMA 9:1 prepared from a 30 wt % dispersion and annealed at 100 °C for 1 h. *Z* is the distance from the surface. The image size is 73 × 73 μm.

observe that the network structure we detected in a freshly formed film persists even after 3 h of annealing. Figures 10−12 have many common features. In all cases, there is no network structure in the regions just below the surface. The mesh size of the network at the surface appears to be smaller than that seen in the deeper sections of the film.

After 10 h of annealing at 100 °C we observe a breakdown of the network structure (Figure 13). The PBMA phase becomes more discernible. Instead of the network strands there are now separate coalesced particles and trains of particles. After 70 h of annealing, the network disappeared, and the contrast in the images becomes stronger, indicating that significant particle coalescence has taken place (Figure 14).

Morphology of Surfactant-Free Blend.. Before removing the surfactant SDS and salts from the dispersions by ion exchange, each latex dispersion was diluted to 5 wt % solids. This dilution was necessary because at higher solids content the viscosity of the ion-exchanged dispersion increases tremendously, making it very difficult to remove the beads of the ion-exchange resin. We found that the dispersion with lower solids content dried slower than the surfactant-containing dispersion with 30 wt % solids. (Note that the two films have different thicknesses, the surfactant-free film is ca. 200 μm thick, and the surfactant-containing film is ca. 400 μm thick). The film formed from the surfactant-free dispersion had a very uniform thickness, and no cracks were seen on the surface.

The film formed from the surfactant-free dispersion has a completely different film structure (as observed by confocal microscopy) than the surfactant-containing film seen in Figure 11. As shown in Figure 15, all images of the surfactant-free film, taken at various depths, look uniformly gray. This result indicates that there is no segregation of PBMA phase and that PBMA latex particles are distributed randomly in the PEHMA matrix.

When a surfactant-free film was annealed at 100 °C for various time intervals and examined by LSCFM, we observe coarsening in the blend structure. Discrete droplets of PBMA phase appear and grow in size with increased annealing time. Examples of the images obtained after 3 and 70 h of annealing are given in Figures 16 and 17.

Table 2 lists the image analysis results for both surfactant-containing and surfactant-free films. Because some of the particles are so small that they cannot be detected, the fraction of the image attributed to the PBMA phase is a useful indicator of the quantity of undetected small particles.

When one examines two-dimensional images of slices through a dispersion of spheres, the area ratio should be equal to the volume ratio of spheres in the matrix. Our PEHMA:PBMA blend is a dispersion of 10 vol % PBMA spheres in a PEHMA matrix. Recall, however, that the fraction of anthracene-labeled PBMA in the blend is 2 wt %. The rest of PBMA phase is phenanthrene-labeled PBMA, which gives no signal in the confocal images. For freshly prepared films one should expect, therefore, to find a PBMA area fraction equal to 0.02. These PBMA particles are too small (120 nm in size) to be seen individually (see Figure 15). We showed by direct nonradiative energy transfer measurements[16] that at 100 °C the coalescence between neighboring anthracene- and phenanthrene-labeled PBMA particles is complete within 20 min. After 3 h of annealing at 100 °C, which is the shortest time used in the present set of experiments, we believe that the anthracene concentration became uniform throughout the PBMA phase. We expect the PBMA area fraction in the images to reflect the total fraction of the PBMA phase, 10%.

When there is no surfactant present in the film, after 3 h of annealing, the average particle diameter is 0.5 μm, and the fraction of the PBMA phase we observe in the image is only 2%. The implication here is that the majority of the PBMA particles or aggregates are so small they cannot be detected. After 10 h of annealing, the particle size and polydispersity do not change, but

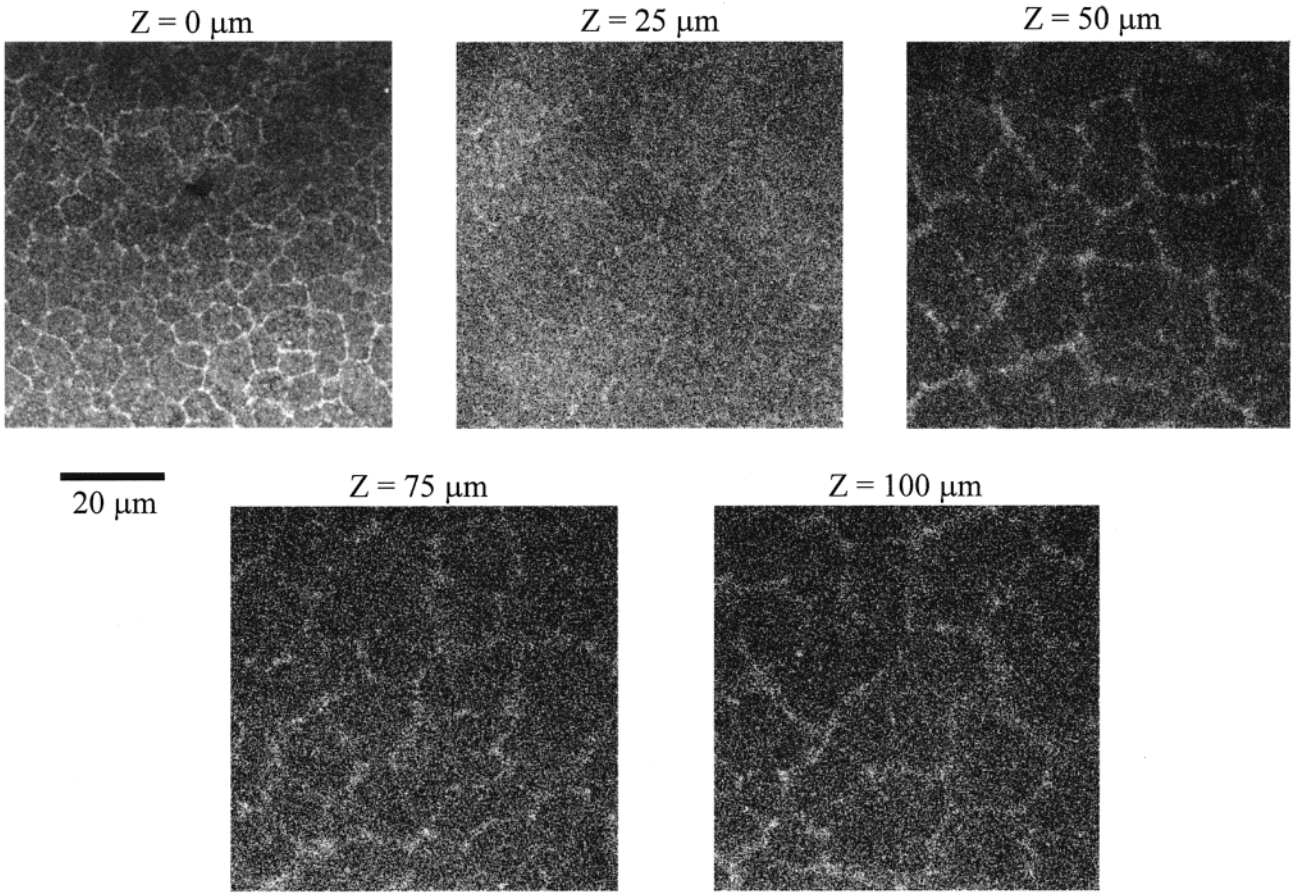

Figure 12. Confocal microscopy images of a surfactant-containing film PEHMA:PBMA 9:1 prepared from a 30 wt % dispersion and annealed at 100 °C for 3 h. *Z* is the distance from the surface. The image size is 73 × 73 μm.

the number of particles detected increases by a factor of 3, and the PBMA area fraction is 4.5%. After 70 h of annealing, both particle size and polydispersity increase, and the area fraction is 9%, indicating that the fraction of PBMA particles with very small sizes decreased considerably.

In surfactant-containing films cast from a 30 wt % dispersion, after 10 h of annealing, the average particle diameter is 0.7 μm, and the PBMA area fraction is 3%. After 70 h of annealing, the average diameter increases slightly (0.8 μm), and the PBMA area fraction is 6.3%. Note that for the same annealing time PBMA domains visualized by LSCFM are larger in the surfactant-containing blend than in surfactant-free blend. We explain this result by the initial aggregation of PBMA in the PEHMA matrix in the presence of surfactant. Some regions of the surfactant-containing film are therefore richer in PBMA latex particles, which facilitates coalescence of PBMA.

Morphology of Surfactant-Containing Blends Cast from Dispersions with Low Solids Content. In the first set of films we examined, PBMA aggregation and the formation of the network structure may be caused either by the presence of surfactant or by the higher initial solids content of the surfactant-containing dispersion. To distinguish between these possibilities, we diluted the surfactant-containing dispersions to 5 and 1 wt % and used them to prepare films. These dispersions were cast onto 1 × 2 cm quartz plates and left to dry uncovered at room temperature. The drying time was long because of the low solids content: the 1 wt % dispersion dried over 2 days. These films after drying have a structure very similar to that described by Feng:[17] a "stadium" structure, with a thick rim around the perimeter of the film and a flat thinner region inside. A cartoon of the film structure is shown in Figure 18. The maximum thickness of the edge was about 60 μm, and in the middle section the films had a thickness of 20−30 μm.

The samples were examined by LSCFM at several different locations, which are marked with the letters a−e in Figure 18. The corresponding images obtained with confocal microscopy are given in Figure 19A−E. A quick glance at the images in Figures 4−19 reveals that there are two types of structures present.

Close to the edge of the film, in a narrow zone about 1 mm thick, we observe a pattern similar to the network structure we detected in the surfactant-containing films prepared from the concentrated dispersion (cf. Figure 19A−C and Figures 10−12). The difference between the two sets of films is that in Figures 10−12 the network is isotropic, whereas in Figure 19A−C there is a distinct alignment of the network threads, which are oriented in the direction perpendicular to the outer edge of the film. Samples were positioned in the microscope sample holder in a way that the *X*-axis of the scanning plane coincided with the long side of the quartz plate and the *Y*-axis coincided with the short side of the quartz plate. That is the reason that the network is aligned differently in the images in Figure 19A−C. The network orientation depends on the position of the region in the film examined (see Figure 18). In Figure 19A the orientation of the network is vertical, and in Figure 19C it is close to horizontal. In Figure 19B the network is aligned at a 45° angle.

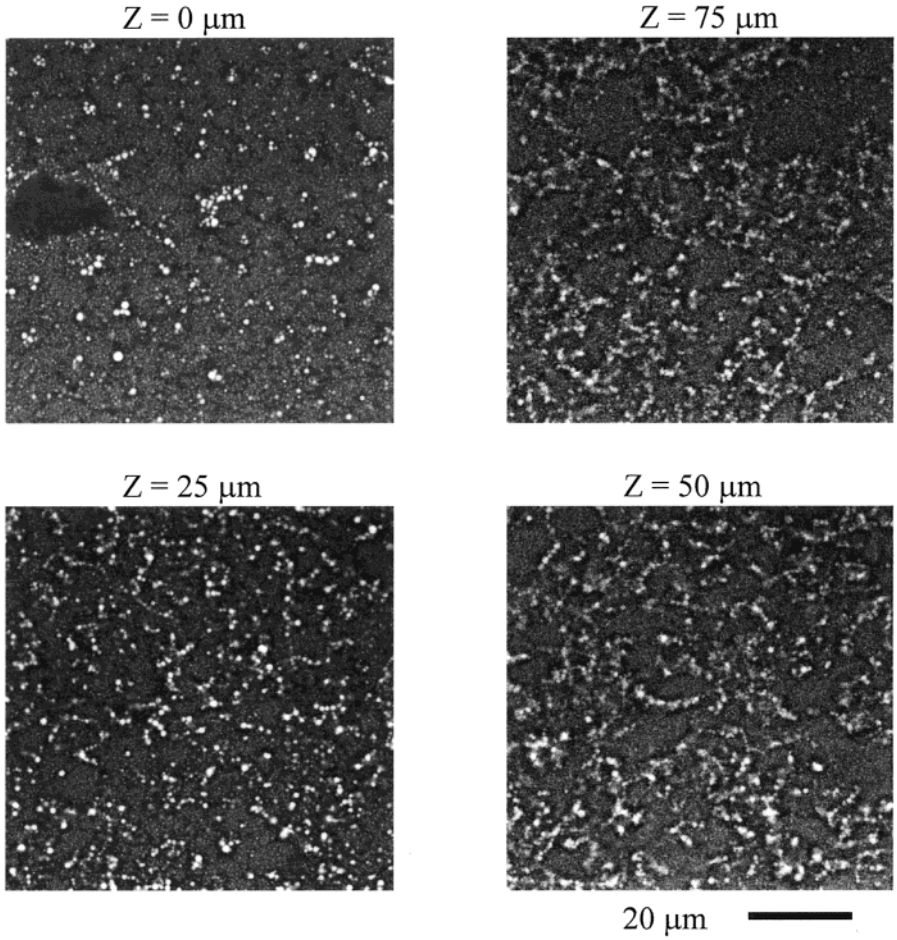

Figure 13. Confocal microscopy images of a surfactant-containing film PEHMA:PBMA 9:1 prepared from a 30 wt % dispersion and annealed at 100 °C for 10 h. *Z* is the distance from the surface. The image size is 73 × 73 μm.

The network is seen only in a narrow region close to the outer film boundary (ca. 300 μm wide). The rest of the film including the thin middle section displays a homogeneous distribution of the dispersed PBMA phase as shown in Figure 19D,E. This type of structure is similar to what we found in surfactant-free films.

Discussion

The results described above demonstrate that for the same composition latex blend we can obtain different film structures depending on whether surfactant is removed from the blend. However, the presence of surfactant is not the only factor influencing the film structure. We showed that by lowering the solids content of the dispersion one could obtain films that are very different from the films cast from the concentrated dispersion. The key to understanding the film morphology is knowing the mechanism of film drying.

First, let us consider the case of surfactant-free films. When surfactant and other ionic species are removed from latex dispersion, the only charges left are associated with the latex particles themselves: in our case, these are the remnants of the initiator at the ends of the polymer chains, $-OSO_3^-$ groups. At low ionic strength, these charges stabilize latex particles by Coulombic repulsion. Under certain conditions (monodisperse latex, high concentration, low ionic strength) a disorder−order transition can take place, in which particles spontaneously arrange themselves into so-called colloidal crystals, where latex particles are regularly spaced in the lattice.[18] Particle movement is severely restricted, and the viscosity of the dispersion increases tremendously. When an ordered dispersion dries, the interparticle distance is gradually reduced until the particles come into close contact. Overall particle concentration increases, and the distribution of particles remains uniform.[19] This is the case of homogeneous drying.

When there are several types of latex particles in a surfactant-free dispersion, a number of different scenarios are possible, depending on the particle size ratio, surface charges, concentration ratio, and so on. A mixed crystal can form, or different particles can form separate phases. In our system, PBMA and PEHMA have similar sizes, 120 and 100 nm, respectively. The number of PBMA particles is relatively small: for every PBMA particle there are 15 PEHMA particles. When surfactant is removed from a 30 wt % dispersion mixture, we observe some signs of crystallization. First of all, the viscosity becomes so high that the dispersion cannot flow, while the analogous surfactant-containing mixture has low viscosity. Second, the ion-exchanged dispersion becomes translucent with a bluish tinge, which is indicative of ordering. The surfactant-containing dispersion is milky white. Comparison of two ion-exchanged dispersions, the PBMA:PEHMA dispersion mixture and the pure PEHMA latex, which is presumed to form a colloidal crystal, reveals no differences in appearance. While these qualitative observations cannot be considered as a proof of crystallization, we can infer that the

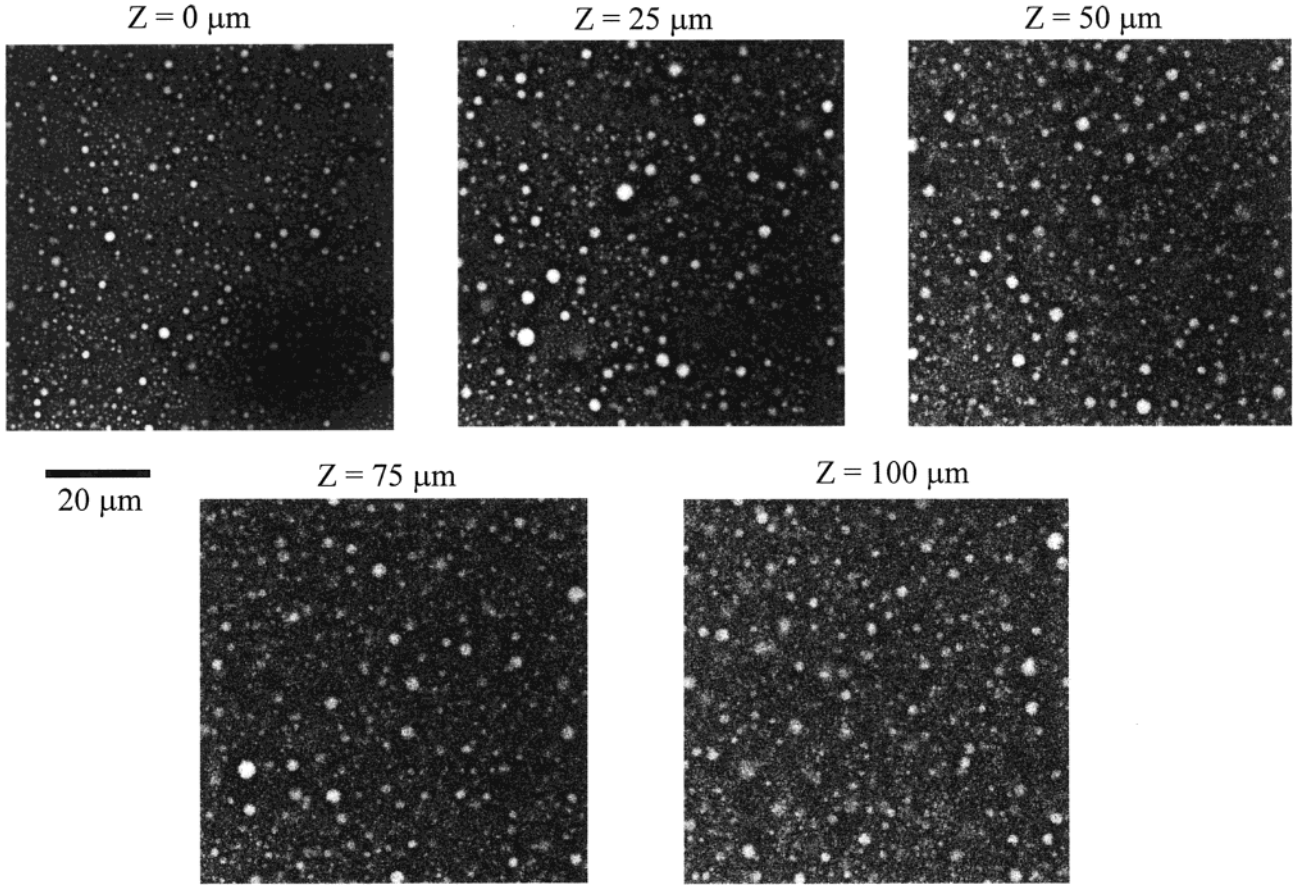

Figure 14. Confocal microscopy images of a surfactant-containing film PEHMA:PBMA 9:1 prepared from a 30 wt % dispersion and annealed at 100 °C for 70 h. *Z* is the distance from the surface. The image size is 73 × 73 μm.

ion-exchanged PBMA:PEHMA latex blend forms a mixed colloidal crystal, with individual PBMA and PEHMA particles located in a common lattice. No phase separation, as detected by confocal microscopy, takes place as the dispersion dries to form a film.

There are other indications that the ion-exchanged dispersion mixture dries homogeneously. There is no skin formation on the surface of the wet film and no edge effects (i.e., no lateral drying and mass transfer to the edges). The dry film is very smooth and has a uniform thickness. In the ion-exchanged mixture PBMA: PEHMA, the final film morphology is determined by the particle arrangement when the system forms an ordered state. Because the system dries homogeneously, this arrangement is retained during drying and carries over to the dry film.

Surfactant-containing films dry in a different way than surfactant-free films. Films cast from low solids content dispersions exhibit lateral drying, characterized by the presence of a drying front that propagates from the outer film edges to the center of the film. Water fluxes inside the film carry the particles to the edges and lift them onto the rim.[20] Because of this lateral transport of particles, the film is thicker close to the edges and thinner in the middle. A large thick planar film of a PBMA−PEHMA blend cast from a concentrated dispersion dries in a slightly different manner. Here we observed skin formation on the surface of the film, which indicates drying with a propagating front in the direction normal to the surface.

A Model for the Formation of Network-like PBMA Structures. There are relatively few reports in the literature of particle segregation in two-component colloidal mixtures. Chu et al.[21] developed a theoretical model of mixtures of large and small particles. For particles with a size ratio on the order of 10, this model predicts aggregation of the large particles due to the attractive depletion force exerted by small particles. Aggregation of large particles results in flocculation and formation of particle clusters. Experimentally, phase separation due to depletion−attraction was observed by Sanyal et al.[22] with a binary mixture of large and small polystyrene particles (0.8 and 4 μm in diameter). They detected flocs of the 4 μm particles by optical microscopy in sedimented dispersion mixtures. No evidence of flocculation was found in single-component samples.

In analyzing their data, Sanyal et al.[22] treated their particles as hard spheres and showed that electrostatic interactions between charge-stabilized polystyrene spheres were effectively screened by ionic impurities in the sample, leading to flocculation. This result is very different from that reported by Ottewill et al.[1a] These authors found that, in the presence of electrostatic repulsion between particles in binary mixtures of large and small particles, it is the smaller particles that form weak clusters. Ottewill et al. studied mixtures of 16.8 and 51 nm polystyrene particles by small-angle neutron scattering (SANS). The latex blend was cleaned by dialysis and then ion exchanged to remove surfactant. Then a small amount of sodium chloride was added to the dispersion mixture. In this system, the authors estimate that there were 43 charges per 16.8 nm particle and 131 charges per 51 nm particle. The neutron scattering results indicated long-range correlations between the small particles caused by their weaker

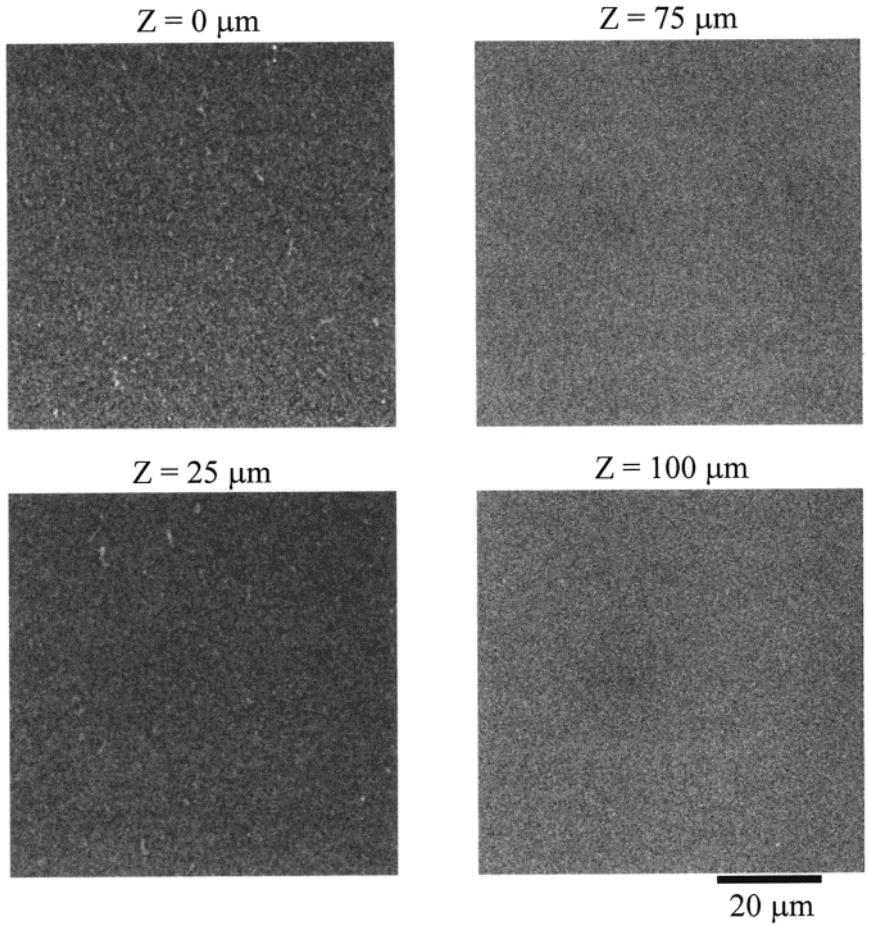

Figure 15. Confocal microscopy images of a freshly formed surfactant-free film PEHMA:PBMA 9:1 prepared from a 5 wt % dispersion. *Z* is the distance from the surface. The image size is 73 × 73 μm.

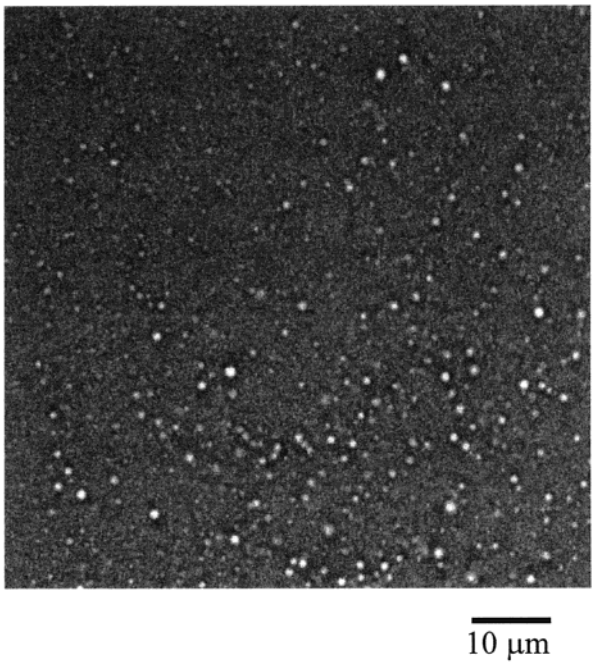

Figure 16. Confocal microscopy image (Z = 10 μm) of a surfactant-free film PEHMA:PBMA 9:1 prepared from a 5 wt % dispersion and annealed at 100 °C for 3 h. *Z* is the distance from the surface. The image size is 73 × 73 μm.

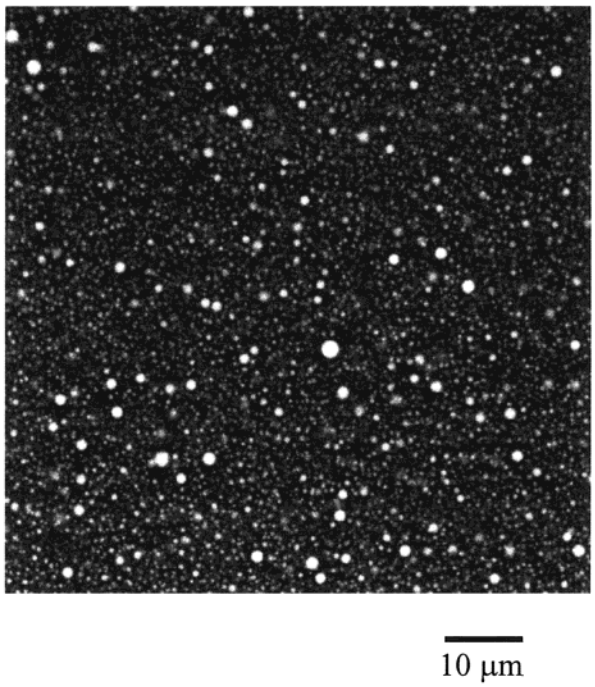

Figure 17. Confocal microscopy image (Z = 10 μm) of a surfactant-free film PEHMA:PBMA 9:1 prepared from a 5 wt % dispersion and annealed at 100 °C for 70 h. *Z* is the distance from the surface. The image size is 73 × 73 μm.

electrostatic repulsion (lower charge). While the system was stable under the low solids condition of this experiment (latex volume fraction ca. 3%), Ottewill et al. comment on the possibility that the weak clusters of small particles may be precursors to phase separation.

Table 2. Results of Image Analysis of Confocal Microscopy Images of PEHMA:PBMA 9:1 Films Annealed at 100 °C[a]

surfactant present	annealing time, h	av particle diameter, μm	PBMA area fraction	count (no. of particles detected)
no	3	0.49 ± 0.13	0.020 ± 0.006	383 ± 86
	10	0.48 ± 0.11	0.045 ± 0.017	1243 ± 389
	70	0.65 ± 0.30	0.091 ± 0.016	1228 ± 229
yes	10	0.73 ± 0.31	0.031 ± 0.006	343 ± 40
	70	0.82 ± 0.46	0.063 ± 0.010	490 ± 150

[a] Averages obtained over 10 optical sections (distance from the surface ranging from 5 to 50 μm).

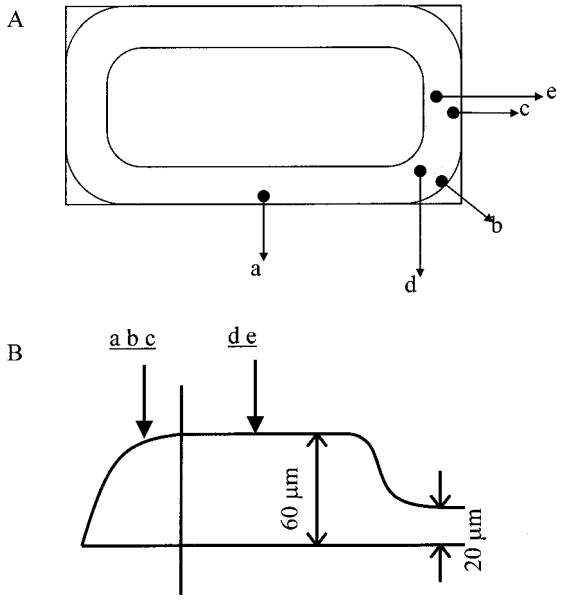

Figure 18. A cartoon representing film structure. (A) Top view of the film. (B) Vertical profile of the edge of the film. Letters a−e represent the positions where samples were examined by confocal microscopy. The corresponding images are given in Figure 19A−C and Figure 20A,B.

More recent results show that even particles with a range of similar sizes can segregate during drying. Rakers et al.[23] studied films formed by particles with a mean diameter of 80 nm (they did not mention the latex chemical composition) and 15% size polydispersity and found that, under certain controlled drying conditions, there was a size-dependent segregation of the particles in the dry film.

Eckersley and Helmer[24] studied blends of hard ($T_g \approx$ 60 °C) and soft ($T_g \approx$ 0 °C) poly(styrene-*co*-butyl acrylate) latex as a function of particle size ratio, R_{soft}/R_{hard}. They found an improvement in mechanical properties of films caused by the addition of hard particles to soft binder latex. They explained their results in terms of percolation theory, which predicts that for a given particle size ratio there is a minimum volume fraction of the hard particles in the blend capable of forming a connecting network of hard particles. The percolation structure is thought to be responsible for improved mechanical properties of the film. This reasoning was supported by examination of the film surfaces by scanning electron microscopy, which showed that the small hard particles were enriched at the film surface. Percolation theory does not consider specific interactions between particles in the dispersion. Rather, it considers random particle packing as a function of particle size and volume fraction.

Chevalier et al.[25] used small-angle neutron scattering to study composite films prepared from a dispersion blend of hard polystyrene particles (45 nm) and soft poly(butyl acrylate) particles (80 nm). They showed that the polystyrene nanospheres formed clusters in a poly(butyl acrylate) matrix and that the polystyrene volume fraction in the clusters was 0.6 no matter what was the overall composition of the dispersion. Wang and Anderson[26] studied films formed by drying dispersion blends of conductive tin oxide particles (60 nm) with various hard and soft polymer nanospheres (60−65 nm). Conductivity studies of the dry films suggested an unusually low percolation threshold, indicating a formation of conductive network at a volume fraction of tin oxide particles of 0.04 or lower. Examination of these films by AFM demonstrated clustering and chaining of the tin oxide particles in the polymer matrices. The authors explain their results in terms of microphase separation of latex particles and clustering of tin oxide particles in the concentrated dispersion during film formation. The two-component films of Wang and Anderson, in which the minor component forms a connected network in a matrix formed by the other component, have a structure very similar to that which we obtain in our films prepared from a blend of PBMA and PEHMA latex particles.

The Role of Surfactant. The fact that network-like structures of PBMA in our system are seen only in blends containing SDS suggests that that the surfactant plays an important role in the network formation mechanism. The presence of surfactant is a major factor affecting the colloidal stability of the dispersion. If the surfactant has a different affinity for the PBMA and PEHMA particles, preferential absorption of the surfactant onto one of the components can modify the balance of attractive and repulsive forces between the particles, for interactions both between particles of the same kind (PBMA−PBMA, PEHMA−PEHMA) and between the two different kinds of particles (PBMA−PEHMA). In our experiments, the SDS is added during the emulsion polymerization reaction, and its primary function is to provide colloidal stability for the latex particles. Some hint of the different tendency of SDS to adsorb onto the surface of these two latex particles is found in Pham's comments[27] about the conditions used to synthesize PEHMA particles. He found that the amount of SDS used to prepare PBMA latex by emulsion polymerization produced coagulum when applied to the preparation of PEHMA latex. To prepare PEHMA particles successfully, it was necessary to add additional SDS to the recipe. Only in this way could he prepare the dispersions that were used in our experiments.

For a deeper understanding of the interaction of these two types of latex with SDS, one needs to examine the adsorption isotherms. The adsorption of SDS onto PEHMA latex particles was studied by Kientz et al.[28] Isotherms were determined by surfactant titration in which the authors monitored the change in the surface tension of the solution. More than 30 years ago, Brodnyan and Kelly[29] used a dialysis method to follow the adsorption of SDS onto PBMA latex particles. Figure 21 shows the corresponding adsorption isotherms for the two latex polymers, replotted from the literature data, and Table 3 lists the adsorption parameters. In Figure 21, the amount of the adsorbed surfactant per latex unit area (Γ, in mol/m^2) is plotted against the free surfactant concentration in the dispersion. One can see that the

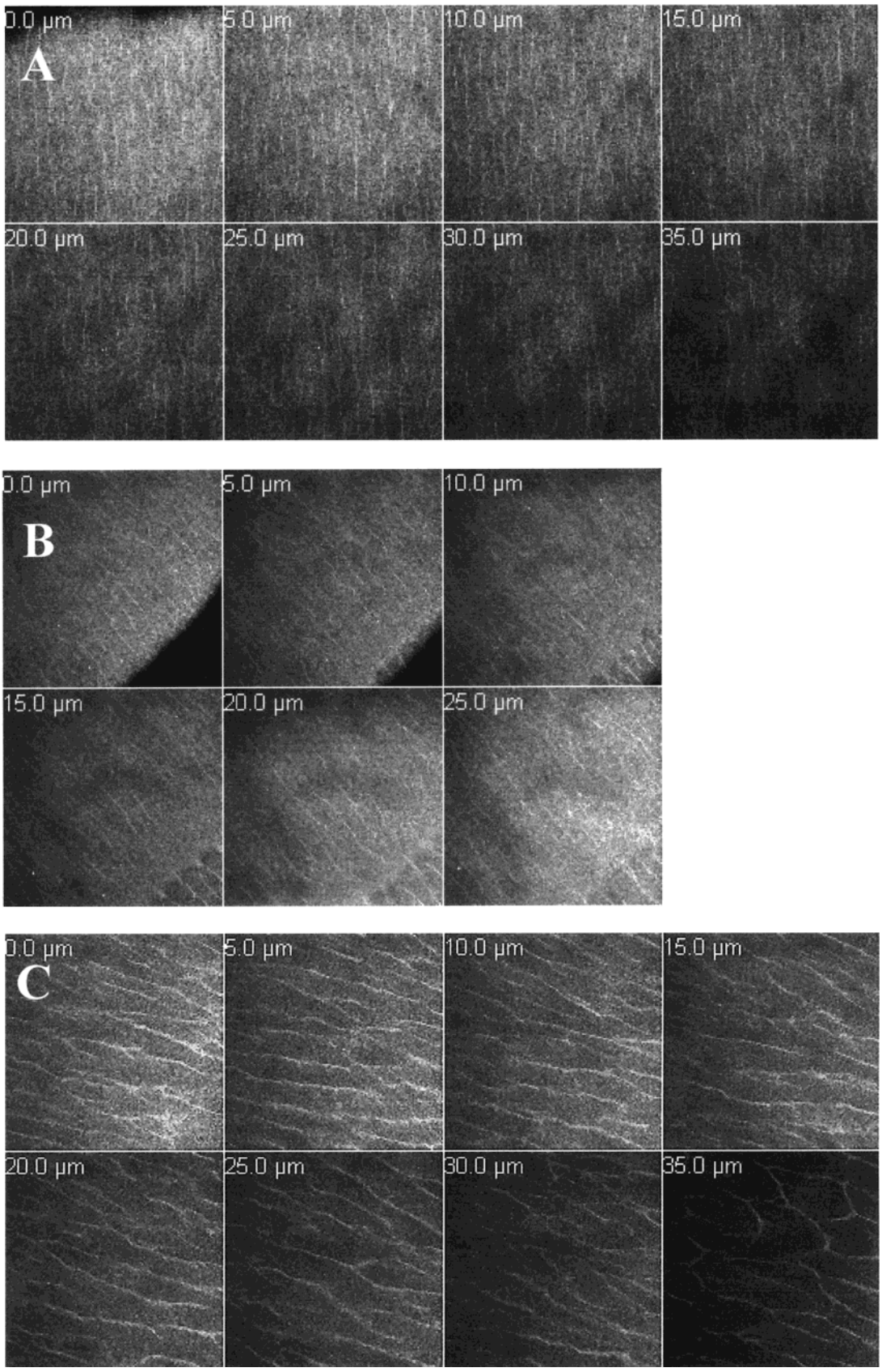

Figure 19. Confocal microscopy images of a freshly formed surfactant-containing film PEHMA:PBMA 9:1 prepared from a 5 wt % dispersion. *Z* is the distance from the surface (shown in each image). The size of each image is 73 × 73 μm. The film thickness for this particular sample is ca. 40 μm. (A) Taken from point a shown in Figure 18, (B) from point b, and (C) from point c.

absorption curves for PEHMA and PBMA are different. In the case of PBMA, the saturation plateau is reached very quickly, when $[SDS]_{free} = 2$ mM, and the adsorption does not change much with a further increase in the free surfactant concentration. This curve resembles a traditional Langmuir isotherm plot. For PEHMA, the

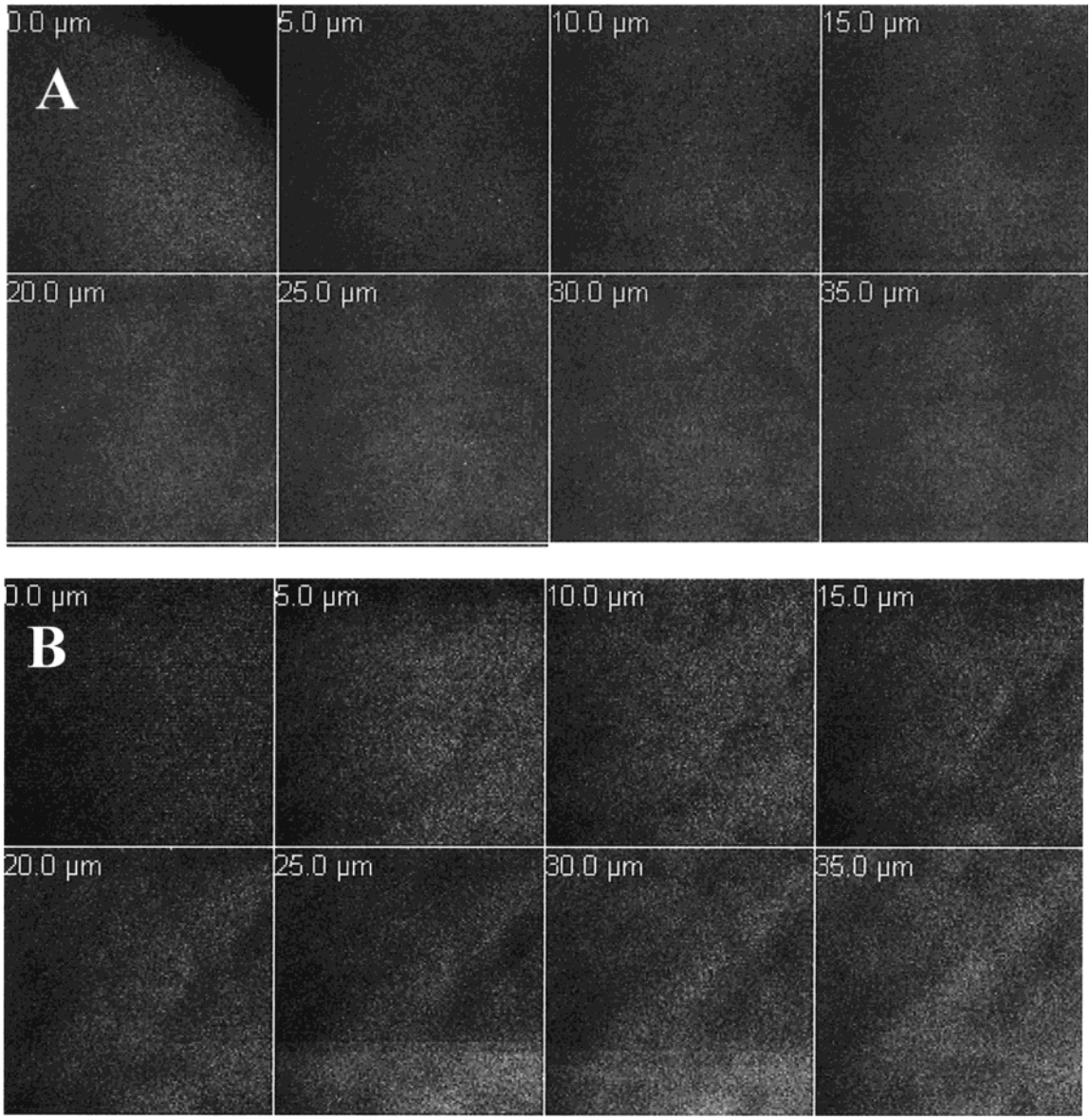

Figure 20. Confocal microscopy images of the same sample shown in Figure 19. (A) Taken from point d shown in Figure 18 and (B) from point e.

Table 3. SDS Adsorption Characteristics for PEHMA and PBMA Latex

latex	PEHMA[a]	PBMA[b]
particle diameter D, nm	99	120
surface area per particle A_1, nm^2	3.14×10^4	4.52×10^4
mass of one particle m_1, g	5.08×10^{-16}	8.82×10^{-16}
latex concentration s, g/L	255	28.3
area per SDS molecule at SDS_{free} = cmc, A_{cmc}, nm^2	0.38	0.59
limiting area per SDS molecule A_0, nm^2	0.16	0.59
adsorption constant K, L/mol	98.2	8000
SDS molecules per particle at SDS_{free} = cmc	82600	76600
coverage ratio (30 wt % solids), %	29	92
SDS molecules per particle at 30 wt % solids	23500	70500
charge density at 30 wt % solids, C/m^2	0.12	0.25

[a] Data from ref 28. [b] Data from ref 29.

adsorption increases strongly with free surfactant concentration, but the plateau is not reached even at the highest possible surfactant concentration, $[SDS]_{free}$ = cmc. In both papers, the authors fitted their data to the Langmuir isotherm equations (1a, 1b). From fits of the data to these equations, one obtains two parameters, the minimum area per surfactant at saturation, A_0, and the adsorption constant K. Γ_0 is the maximum amount of surfactant adsorbed. N_{Avo} is Avogadro's constant.

$$\frac{\Gamma}{\Gamma_0} = \frac{Kc_{free}}{1 + Kc_{free}} \tag{1a}$$

$$\Gamma_0 = \frac{1}{N_{Avo}A_0} \tag{1b}$$

Another important parameter is the area per surfactant when the free surfactant concentration equals the cmc, A_{cmc}. This parameter, rather than Γ_0, determines the maximum amount of surfactant concentration that can actually be adsorbed to the latex. The reason for this distinction is that the free surfactant concentration can never exceed the cmc. Values of A_{cmc} are relatively easy to determine experimentally. As a consequence, these values are known more accurately than values of

the absorption constant K. One needs to have data over the entire isotherm to properly calculate K. From this perspective, we are concerned about the difference in the shape of the adsorption isotherms for SDS on the two rather similar latex particles. Fitting the two curves in Figure 21 to eq 1 leads to a value of K for PEHMA 8 times smaller than that for PBMA (Table 3). This fitting process also leads to a value of A_0 for SDS on PEHMA (16 Å^2) which is almost a factor of 4 smaller than that (59 Å^2) for SDS on PBMA. In summary, fitting the curves in Figure 21 to a Langmuir isotherm yields parameters which suggest that at low surfactant concentration SDS binds more strongly to PBMA than to PEHMA. At high surfactant concentration, the situation is reversed, with a significantly smaller area per surfactant for SDS on the surface of PEHMA than on PBMA. In terms of A_{cmc} values, one finds 59 Å^2 per SDS molecule on the surface of a PBMA latex particle, compared to 38 Å^2 for SDS on the surface of a PEHMA latex particle.

With these adsorption parameters, we can calculate the amount of SDS adsorbed onto the PBMA particles and PEHMA particles in our dispersion mixture as well as the nominal charge density for the two types of particles. At 29% solids in the dispersion mixture containing 90% of PEHMA and 10% of PBMA, the total SDS concentration $C_{SDS\ total} = 25$ mM. The concentration of the surfactant bound to the latex c_{bound} (in mol/L) is defined by the following equation:

$$c_{bound} = \frac{\Gamma A_1 s}{m_1} \tag{2}$$

where Γ is the amount of the adsorbed surfactant in mol/m^2, A_1 and m_1 are the area and the mass of one latex particle, and s is the latex concentration in the dispersion mixture in g/L. Assuming after Stubbs et al.[30] that SDS adsorbs onto PBMA and PEHMA particles independently, and combining eqs 1 and 2, we arrive at the following expression:

$$c_{bound} = \left[\frac{A_1 s}{m_1 N_{Avo} A_0}\frac{Kc_{free}}{1 + Kc_{free}}\right]_{PEHMA} + \left[\frac{A_1 s}{m_1 N_{Avo} A_0}\frac{Kc_{free}}{1 + Kc_{free}}\right]_{PBMA} \tag{3}$$

Taking into account that $c_{total} = c_{bound} + c_{free}$ and solving eq 3 for c_{free}, we obtain $c_{free} = 1.4$ mM, which corresponds to 94% adsorption. Knowing c_{free}, we can calculate the amount of SDS per latex particle for both the PBMA and PEHMA latex, which gives us the value of the nominal charge per PBMA and PEHMA particle. We find that the number of SDS molecules per PBMA particle is 3 times higher than that for each PEHMA particle. The nominal charge density, expressed as the total charge divided by the particle surface area, is 2 times larger for PBMA particles than for PEHMA particles.

The larger surface charge associated with the larger number of surfactant molecules adsorbed onto the PBMA particles results in increased colloidal stability of PBMA particles compared to the PEHMA particles. When the film dries, the solids content of the dispersion increases and so does the concentration of all ionic species (buffer and surfactant) present in the dispersion. The increase in the ionic strength leads to a diminished

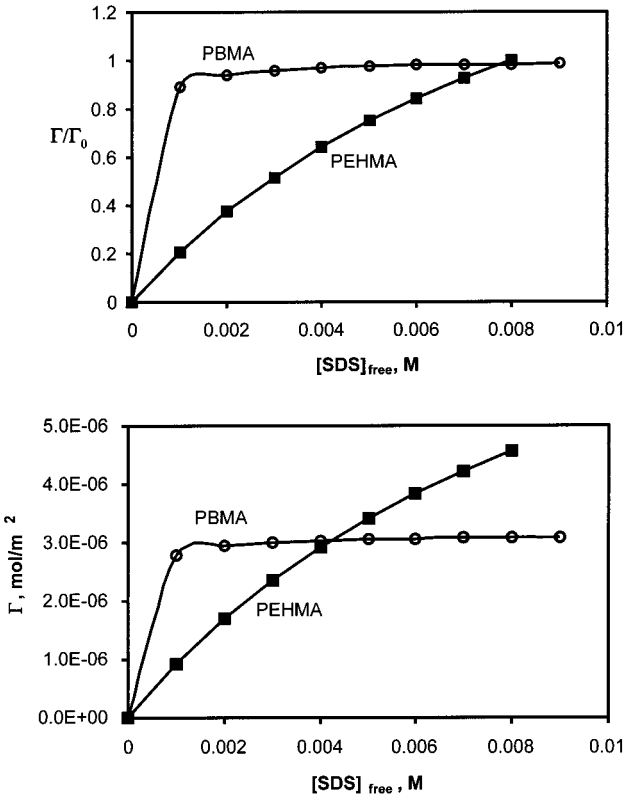

Figure 21. SDS adsorption onto PEHMA and PBMA latex. Top: coverage ratio. Bottom: amount of SDS adsorbed per latex unit surface area in mol/m^2. PBMA data are reproduced from ref 24, and PEHMA data are reproduced from ref 23.

repulsion between the charged latex particles (the so-called screening effect). It is well-known that addition of a strong electrolyte to a charge-stabilized colloidal dispersion will lead to flocculation. Coagulation will occur when the concentration of the electrolyte equals the critical coagulation concentration.

In our dispersion mixture, the increase in the ionic strength is not so significant as to cause rapid precipitation. Rather, we believe that the effect is more subtle: the repulsion between the latex particles in the dispersion decreases more strongly for the surfactant-poor PEHMA particles than for the more highly charged PBMA particles. We presume that PEHMA latex is more likely to flocculate at earlier stages in the drying process, when the particles are still not in close contact. Some of the flocs may be mixed, i.e., containing both PBMA and PEHMA particles. At close contact, PBMA particles occupy the space around the PEHMA flocs and form a connected network. We show this process schematically in Figure 22.

Our interpretation of the segregation in the surfactant-containing PBMA and PEHMA latex mixtures was based on SDS adsorption data obtained from the literature.[28,29] These data allowed us to calculate the particle charge for both components. Determination of a surfactant adsorption isotherm is a delicate experiment subject to a large uncertainty in the data at low free surfactant concentrations, which have the strongest influence on the value of adsorption constant K. The data we employ were determined by different experimental methods. While we have no grounds to doubt the two sets of data, we are puzzled about why the PBMA and PEHMA particles, with similar chemical structures, show such differences in the SDS adsorption

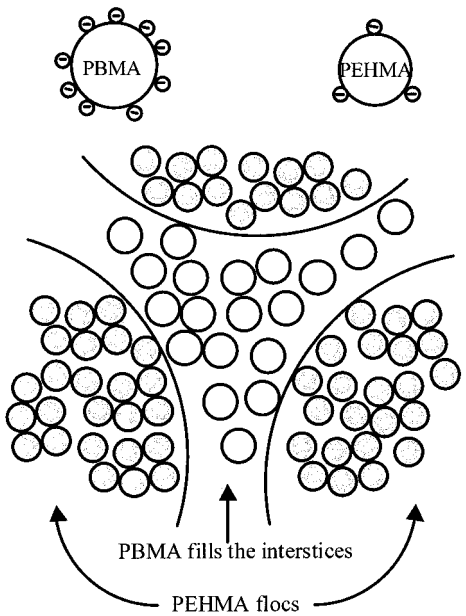

Figure 22. A scheme of aggregation in PEHMA:PBMA 9:1 dispersion mixture. The difference in surface charge causes the PEHMA and PBMA to segregate.

isotherms. Nor it is clear why the more hydrophobic PEHMA surface has an adsorption constant 8 times smaller than that for PBMA or why the adsorption onto PEHMA does not reach saturation, as one might expect for Langmuir adsorption (see data in Table 3 and Figure 21).

The amount of SDS present in our dispersion mixture is rather small, 2.3 wt % in the dry film. At this level of surfactant, the concentration of free surfactant in the dispersion is very low, and the uncertainty in the adsorption data is high. When the concentration of free surfactant is equal to the cmc (this amount of SDS would be about 7 wt % in the dry film), the charges on PBMA and PEHMA particles would be very similar (see Table 3), although in this case the charge density would be higher on the PEHMA particles (0.42 C/m^2) than on the PBMA particles (0.27 C/m^2). Therefore, it would be very interesting to examine film morphology for this blend for different surfactant concentrations in the dispersion.

Knowledge of the drying mechanism can help us understand the segregation of PBMA and PEHMA and the formation of network-like structures we observed by confocal microscopy. In films cast from the low solids dispersion, we found that the network is aligned in the direction of the drying front propagation (perpendicular to the edges of the film). The orientation of the structures at the edge of the film suggest that aggregated structures of PBMA form in this region. The flow of water toward the edges of the film acts to align these aggregates in the direction of the flow. As PEHMA and PBMA particles are carried with the water flux to the drying edge, they are more likely to join the particles of the same kind. PEHMA is a soft latex, so that its particles can be easily deformed to fill the space under the action of the capillary forces. PBMA particles cannot be deformed as easily, so that they probably are "squeezed out" into separate domains. This is also beneficial for the drying efficiency of the film. Coalescence of PEHMA particles leads to a decrease in the diameter of the pores through which water can diffuse. PBMA particles are unable to coalesce and therefore retain their pores until the later stages of film formation, when PEHMA diffuses around particles of PBMA, filling all empty spaces. We can consider network threads in Figure 15 as aqueducts, channels for water diffusion. It is not clear why the network structure forms only at the edge of the film. Maybe, as the rate of the water loss decreases in the central area of the film, the drying becomes more homogeneous.

In films cast from a concentrated dispersion, there is no specific lateral direction for the particle transport, and the network has no apparent direction.

To conclude this section, we return to the films formed from the latex blend at 5 wt % solids in the presence of SDS. These are the films shown in Figure 19 which exhibit white lines of PBMA aggregates at the edges of the film, all oriented perpendicular to the edge. Two features of this structure are unusual: the selective aggregation of the PBMA particles at the edge of the film and the structure of the aggregates as chains oriented perpendicular to the edge.

From the work of Denkov et al.,[20] we understand a great deal about the nature of the drying mechanism and the forces involved that lead to the "stadium"-like architecture of a flat film surrounded by an elevated ridge. When the dispersion is spread on a substrate, it dried first where the liquid film is thinnest. If the contact angle at the edge of the dispersion is less than 90°, this occurs at the film edge. The deposition of solid at the edge provides an enhanced surface area where water evaporation is faster than from the flat surface of the "lake" of dispersion in the interior. In this situation we can imagine that there is an increase in ionic strength in the fluid at the edge, promoting flocculation of PEHMA as described above. At the same time, the flux of water toward the edges of the film lifts particles onto the rim which forms at the film edge. It is this flux which drives the orientation of the PBMA particles caught between the domains enriched in PEHMA.

Conclusion

In this paper we described the results of the study of film morphology, by AFM and LSCFM, for films prepared from a blend of two latex dispersions. The films were composed from 90 wt % of PEHMA and 10 wt % of PBMA. We observed that these films have different structures depending on the presence or absence of the surfactant SDS and solids content of the dispersion. We relate these differences to differences in the drying mechanisms for the film. In the presence of surfactant, we observe network-like structures formed by PBMA particles in a matrix of PEHMA. The segregation of PBMA and PEHMA particles can be explained by differences in the surfactant adsorption onto PBMA and PEHMA particles.

Acknowledgment. The authors thank NSERC Canada for the support of this research and Imaging Research Inc. for the image analysis software AIS.

References and Notes

(1) (a) Ottewill, R. H.; Hanley, H. J. M.; Rennie, A. R.; Straty, G. C. *Langmuir* **1995**, *11*, 3757−3765. (b) Clarke, S. M.; Rennie, A. R.; Ottewill, R. H. *Langmuir* **1997**, *13*, 1964−1969. (c) Zhu, J. X.; Rogers, R.; Meyer, W.; Ottewill, R. H.; Russell, W. B.; Chaikin, P. M. *Nature* **1997**, *387*, 883−885.

(2) (a) Geurts, J. M.; Lammers, M.; German, A. L. *Colloids Surf. A* **1996**, *108*, 295−303. (b) Peters, A. C. I. A.; Overbeek, G.

C.; Buckmann, A. P. J.; Padget, J. C.; Annable, T. *Prog. Org. Coat.* **1996**, *29*, 183−194.
(3) Vorobyova, O.; Winnik, M. A. *J. Polym. Sci., Part B: Polym. Phys*., submitted for publication.
(4) Sawyer, L. C.; Grubb, D. T. *Polymer Microscopy*, 2nd ed.; Chapman and Hall: London, 1996.
(5) (a) Li, L.; Sosnowski, S.; Chaffey, C. E.; Balke, S. T.; Winnik, M. A. *Langmuir* **1994**, *10*, 2495−2497. (b) Kumacheva, E.; Li, L.; Winnik, M. A.; Shinozaki, D. M.; Cheng, P. C. *Langmuir* **1997**, *13*, 2483−2489. (c) Ribbe, A. E.; Hashimoto, T.; Jinnai, H. *J. Mater. Sci.* **1997**, *31*, 5837−5847.
(6) Zhu, S.; Jin, X.; Chen, L.; He, Q. *Sci. China B* **1998**, *41*, 549−555.
(7) Bhawalkar, J. D.; Swiatkiewicz, J.; Prasad, P. N.; Pan, S. J.; Shih, A.; Samarabandu, J. K.; Cheng, P. C.; Reinhardt, B. A. *Polymer* **1997**, *38*, 4551−4555.
(8) Pham, H. H.; Farinha, J. P. S.; Winnik, M. A. *Macromolecules* **2000**, *33*, 5850−5862.
(9) Feng, J.; Winnik, M. A. *Macromolecules* **1997**, *30*, 4324.
(10) Phenanthrene-labeled PBMA does not contribute to the signal in confocal microscopy images. We kept the blend composition the same as in our parallel studies of droplet coalescence in these blends.
(11) Juhué, D.; Wang, Y.; Lang, J.; Leung, O.-M.; Goh, C.; Winnik, M. A. *J. Polym. Sci., Part B: Polym. Phys.* **1995**, *33*, 1123−1133.
(12) Lam, S.; Hellgren, A. C.; Sjöberg, M.; Holmberg, K.; Schoonbrood, H. A. S.; Unzué, M. J.; Asua, J. M.; Tauer, K.; Sherrington, D. C.; Montoya Goni, A. *J. Appl. Polym. Sci.* **1997**, *66*, 187−198.
(13) Tzitzinou, A.; Jenneson, P. M.; Clough, A. S.; Keddie, J. L.; Lu, J. R.; Zhdan, P.; Treacher, K. E.; Satguru, R. *Prog. Org. Coat.* **1999**, *35*, 89−99.
(14) Amalvy, J. I.; Soria, D. B. *Prog. Org. Coat.* **1996**, *28*, 279−283.
(15) Agarwal, N.; Farris, R. J. *J. Appl. Polym. Sci.* **1999**, *72*, 1407−1419.
(16) Vorobyova, O. Ph.D. Thesis University of Toronto, 2000.
(17) Feng, J. Ph.D. Thesis University of Toronto, 1996.
(18) Fitch, R. M. *Polymer Colloids: A Comprehensive Introduction;* Academic Press: London, 1997; Chapter 9.
(19) (a) Chevalier, Y.; Pichot, C.; Graillat, C.; Joanicot, M.; Wont, K.; Maquet, J.; Lindner, P.; Cabane, B. *Colloid Polym. Sci.* **1992**, *270*, 806−821. (b) Joanikot, M.; Wong, K.; Maquet, J.; Chevalier, Y.; Pichot, C.; Graillat, C.; Lindner, P.; Rios, L.; Cabane, B. *Prog. Colloid Polym. Sci.* **1990**, *81*, 175−183.
(20) (a) Denkov, N. D.; Velev, O. D.; Kralchevsky, P. A.; Ivanov, I. B.; Yoshimira, H.; Nagayama, K. *Langmuir* **1992**, *8*, 3183−3190. (b) Deegan, R. D.; Bakajin, O.; Dupont, T.; Huber, G.; Nagel, S.; Witten, T. A. *Nature* **1997**, *389*, 827−829. (c) Winnik, M. A. *Current Opin. Colloid Interface Sci.* **1997**, *2*, 192−199.
(21) Chu, X. L.; Nikolov, A. D.; Wasan, D. T. *Langmuir* **1996**, *12*, 5004−5010.
(22) Sanyal, S.; Easwar, N.; Ramaswamy, S.; Sood, A. K. *Europhys. Lett.* **1992**, *18*, 107−110.
(23) Rakers, S.; Chi, L. F.; Fuchs, H. *Langmuir* **1997**, *13*, 7121−7124.
(24) Eckesley, S. T.; Helmer, B. J. *J. Coat. Technol.* **1997**, *69*, 97−107.
(25) Chevalier, Y.; Hidalgo, M.; Cavaillé, J.-Y.; Cabane, B. *Macromolecules* **1999**, *32*, 7887−7896.
(26) Wang, Y.; Anderson, C. *Macromolecules* **1999**, *32*, 6172−6179.
(27) Pham, H.; Winnik, M. A. *J. Polym. Sci., Part A: Polym. Chem.* **2000**, *38*, 855−869.
(28) Kientz, E.; Danicher, L.; Lambla, M.; Holl, Y. *Polym. Int.* **1993**, *31*, 297−304.
(29) Brodnyan, J. G.; Kelley, E. L. *J. Polym. Sci., Part C* **1969**, *27*, 263−273.
(30) Stubbs, J. M.; Durant, Y. G.; Sundberg, D. C. *Langmuir* **1999**, *15*, 3250−3255.

MA001080U